buildings

MDPI

Article

Research on the Method of Absolute Stress Measurement for Steel Structures via Laser Ultrasonic

Hongsong Tian [1], Yujiang Kong [1], Bin Liu [1], Bin Ouyang [1], Zhenfeng He [2,3,*] and Leng Liao [2,3]

[1] Guizhou Bridge Construction Group Co., Ltd., Guiyang 550001, China; thongsong96@163.com (H.T.); kyj2969@163.com (Y.K.); liubin-xinguang@126.com (B.L.); gqzgb@gzql.cn (B.O.)
[2] State Key Laboratory of Mountain Bridges and Tunnel Engineering, Chongqing Jiaotong University, Chongqing 400074, China
[3] School of Civil Engineering, Chongqing Jiaotong University, Chongqing 400074, China
* Correspondence: 631501010724@mails.cqjtu.edu.cn

Abstract: Accurate measurement of the stress in steel structures is crucial for structural health monitoring. To achieve this goal, a novel technique, the laser ultrasonic technique, was used in absolute stress measurement in this study. The feasibility of this technique has been verified through theoretical analysis and finite element (FE) analysis. A stress measurement experiment in steel specimens was conducted and the relationship between ultrasonic relative wave velocity and stress was explored. The results revealed that there is a similar linear correlation between the ultrasonic relative wave velocity and absolute stress. The stress can be obtained based on ultrasonic relative wave velocity. According to the stress measurement results, it was found that the absolute error between the measured stress and theoretical stress was largest when the stress level was low, and that the measured error of stress gradually decreased with increases in the applied stress. The relative error between the measured stress and the theoretical stress was within 10% when the stress was higher than 100 MPa. This further verifies the reliability of the laser ultrasonic technique under high-stress conditions. Additionally, the impact of temperature and surface roughness on stress measurement was analyzed. The stress error in stress measurement increased similarly linearly with the increase in temperature and increased non-linearly with the increase in roughness. The corresponding compensation methods were proposed to effectively improve the accuracy of measurement.

Keywords: absolute stress measurement; steel structure; laser ultrasonic; influence factors

Citation: Tian, H.; Kong, Y.; Liu, B.; Ouyang, B.; He, Z.; Liao, L. Research on the Method of Absolute Stress Measurement for Steel Structures via Laser Ultrasonic. *Buildings* **2024**, *14*, 602. https://doi.org/10.3390/buildings14030602

Academic Editor: Harry Far

Received: 29 January 2024
Revised: 21 February 2024
Accepted: 21 February 2024
Published: 23 February 2024

1. Introduction

Steel structures are renowned for their robustness and superior seismic capabilities, making them a popular choice in constructing large-span bridges; however, they are vulnerable to significant damage from loads such as earthquakes, leading to potential safety risks. To maintain their operational integrity and prevent accidents, it is crucial to regularly assess the stress state of these bridges, as this directly reflects their structural health [1–4]. Traditional stress measurement techniques fall into two categories: destructive and non-destructive testing. Destructive testing, which can harm the integrity of the bridge, is not ideal for regular checks [5,6]. Consequently, the non-destructive testing/dynamic monitoring approaches of stress in steel structures, including ultrasonic and magnetic flux leakage testing, along with the corresponding artificial intelligence algorithms, have become the primary focus of research [7–10]. Ultrasonic testing, in particular, has widespread application, but its effectiveness is hampered by the need for direct contact and couplants, which can affect measurement sensitivity and accuracy [11,12]. In addition, the size of the transducers further limits the precision and resolution of this method. An innovative solution to these challenges is the laser ultrasonic technique. This technique employs lasers to generate ultrasonic waves without physical contact, bypassing the limitations associated with couplants and transducers. Suitable for use in high-temperature or corrosive settings,

the laser ultrasonic technique offers enhanced precision and spatial resolution, positioning it as a superior alternative in assessing the health of steel bridges.

White [13] et al. demonstrated the feasibility of exciting ultrasonic waves in solids using pulsed lasers, by constructing a one-dimensional theoretical model of the response of a material to laser excitation. Subsequent studies on laser ultrasonic technology used in stress measurement have achieved a series of developments. Zhan et al. [14–16] determined the acoustoelastic coefficients for TC4 titanium alloy and 7075 aluminum alloy specimens using a prestress loading method, and calculated the transverse and longitudinal residual stresses of the test pieces using the acoustoelastic equation, discussing the impact of welding parameters on residual stresses. Xue et al. [17] conducted experiments on stress detection in aluminum alloy under different tensile loads using laser ultrasonics. The experimental results were similar to those obtained using the X-ray method, demonstrating the high precision and accuracy of the laser ultrasonic detection method in measuring stress. Ye et al. [18] proposed a method for measuring residual stress on the surface/subsurface of welded components. Pan et al. [19] explored the significant quantitative relationship between laser ultrasonic velocity and residual stress in high-temperature alloys and verified the method using X-ray detection results, realizing the quantitative detection of alloy stress. Ji et al. [20,21] found a positive correlation between the relative velocity of laser ultrasonic guided waves and tension, and a negative correlation with group velocity, through experiments. Qian et al. [22] conducted a detection on the variation of residual stress on the shot-peened surface of the K417G turbine disk, using laser ultrasonic technology and X-ray methods. The results showed that the changes detected by both methods were consistent, verifying that laser ultrasonic technology can effectively identify the trend of residual stress changes. The research of He et al. [23] indicated that ultrasonic surface waves propagating in the direction of the principal stress are most reasonable for assessing the residual principal stress in 45# steel, and that there is a significant negative correlation between the peak amplitude of the ultrasonic wave and the stress. Santhakumar et al. [24] proposed a theoretical calculation model for the distribution of residual stress based on the laser ultrasonic detection method, achieving accurate detection of the residual stress distribution in titanium alloys. These studies have shown the great potential of laser ultrasonic detection technology in stress measurement. In summary, laser ultrasonic detection technology is primarily used to characterize residual stress in metals, but there are few studies on the detection of absolute stress in steel structures. Therefore, in this work, a method for detecting absolute stress in steel structures based on laser ultrasonics is proposed, drawing on the application of the method in the detection of metal residual stress. The laser ultrasonic wave speed variation characteristics of loading steel structures were explored based on theory, simulation, and experiments. On this basis, the effective detection of absolute stress in steel structures based on laser ultrasonics was achieved. The workflow is shown in Figure 1.

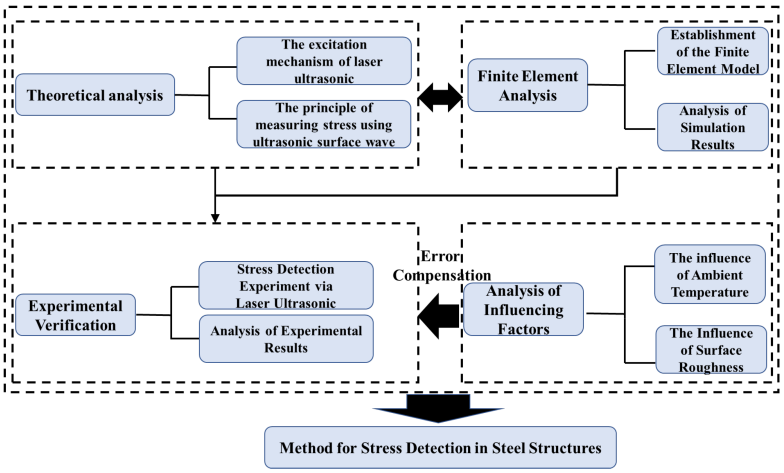

Figure 1. Schematic diagram of the workflow.

2. Theoretical Background

2.1. The Excitation Mechanism of Laser Ultrasonics

When the surface of a solid material is irradiated by a pulsed laser, the absorbed laser energy is converted into thermal energy. A portion of the energy is absorbed by the material and propagates from the surface into the interior, converting into thermal energy. This process rapidly increases the surface temperature of the material through heat conduction, forming a transient, uneven temperature field. Thus, the area of the material exposed to the laser radiation undergoes thermal expansion, which in turn generates thermal stress. The thermal stress propagates to the surrounding medium in the form of a transient pulse so that the ultrasonic waves are excited on the surface of the solid material. The principle of the excitation with laser ultrasonics is shown in Figure 2.

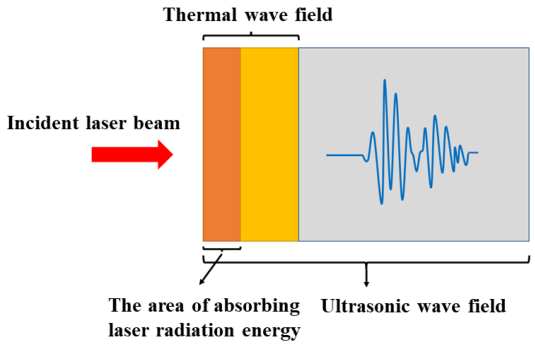

Figure 2. The principle of the excitation with laser ultrasonics.

The theory of laser ultrasonics is based on the thermoelastic mechanism. If the incident laser energy increases the temperature of the material without causing a phase change, this results in thermal expansion and, consequently, the generation of thermoelastic stress. This stress excites ultrasonic waves at the surface or within the material. The thermoelastic stress and strain induced by temperature changes can be solved using the principles of thermoelasticity. There are three fundamental equations in thermoelasticity, which are as follows [25]:

Equation of motion:

$$\sigma_{ij,j} + f_i = \rho \frac{\partial u_i^2}{\partial t} \tag{1}$$

Strain displacement equation:

$$\varepsilon_{ij} = \frac{1}{2}(u_{i,j} + u_{j,i}) \tag{2}$$

Constitutive equation for isotropic materials:

$$\sigma_{ij} = \lambda \delta_{ij} \varepsilon_{kk} + 2\mu \varepsilon_{ij} - \alpha(3\lambda + 2\mu)\delta_{ij} T \tag{3}$$

where i,j = 1,2,3, u_i represents the displacement component, ε_{ij} represents the component of the strain tensor, σ_{ij} represents the component of the stress tensor, ρ is the density of materials, f_i is the external force applied, T represents the increase in temperature, λ and μ are the Lamé constants, δ_{ij} is the unit tensor, α is the coefficient of thermal expansion.

In an isotropic solid, by combining the motion equation shown in Equation (1), the strain-displacement equation shown in Equation (2), and the constitutive equation shown in Equation (3), the Navier–Stokes equation can be derived as follows:

$$\mu U_{i,kk} + (\lambda + \mu) U_{k,ki} - \alpha(3\lambda + 2\mu) T_i + f_i = \rho \ddot{U}_i \tag{4}$$

For isotropic materials, the thermoelastic coupling equations can be simplified when the external forces and internal heat sources in the material are neglected:

$$\mu\nabla^2 U + (\lambda+\mu)\nabla\nabla\cdot U - \alpha(3\lambda+2\mu)\nabla T = \rho\ddot{U} \tag{5}$$

where U represents the displacement vector and T denotes the increase in temperature. Considering the scenario where a pulsed laser with a Gaussian distribution irradiates the surface of an isotropic solid, the boundary conditions on the upper and lower surfaces of the material are free in the normal direction, as shown in Equation (6):

$$n\cdot[\sigma - \alpha(3\lambda+2\mu)T(r,z,t)I] = 0 \tag{6}$$

where I represents the identity tensor, σ denotes the stress tensor, and n is the unit vector perpendicular to the surface of the material. Additionally, the following initial conditions should be satisfied:

$$U(r,z,t)|_{t=0} = \left.\frac{\partial U(r,z,t)}{\partial t}\right|_{t=0} = 0 \tag{7}$$

Finally, the ultrasonic wave displacement field at each point within the material can be obtained by simultaneously solving Equation (5) through Equation (7).

2.2. The Principle of Measuring Stress Using Ultrasonic Surface Wave

Due to the nature of the ultrasonic surface waves propagating solely along the surface of the material, their amplitude is minimally affected by the propagation distance, resulting in a high signal-to-noise ratio. The ultrasonic surface waves are highly effective in measuring absolute stress by using this characteristic. For isotropic solids, Hughes and Kelly measured the third-order elastic constants of an object based on the nonlinear elasticity theory proposed by Murnaghan [26], and the relationship between ultrasonic wave velocity and stress in isotropic materials under stress was formulated.

For an isotropic solid under stress, the principal stress directions can be represented using a coordinate system, as shown in Figure 3. The relationship between the velocity of different modes of ultrasonic waves and stress is given by Equation (8) [27].

$$\begin{cases} \rho_0 V_{11}^2 = \lambda + 2\mu + \frac{\sigma_{11}}{3\lambda+2\mu}\left[\frac{\lambda+\mu}{\mu}(4m+4\lambda+10\mu)+\lambda+2l\right] \\ \rho_0 V_{12}^2 = \rho_0 V_{13}^2 = \mu + \frac{\sigma_{11}}{3\lambda+2\mu}\left[m+\frac{\lambda n}{4\mu}+4\lambda+4\mu\right] \\ \rho_0 V_{22}^2 = \rho_0 V_{33}^2 = \lambda + 2\mu + \frac{\sigma_{11}}{3\lambda+2\mu}\left[2l-\frac{2\lambda}{\mu}(m+\lambda+2\mu)\right] \\ \rho_0 V_{21}^2 = \rho_0 V_{31}^2 = \mu + \frac{\sigma_{11}}{3\lambda+2\mu}\left[m+\frac{\lambda n}{4\mu}+\lambda+2\mu\right] \\ \rho_0 V_{23}^2 = \rho_0 V_{32}^2 = \mu + \frac{\sigma_{11}}{3\lambda+2\mu}\left[m-\frac{\lambda n}{2\mu}-\frac{n}{2}-2\lambda\right] \end{cases} \tag{8}$$

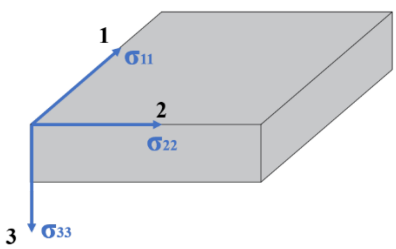

Figure 3. The direction of principal stress.

In this equation, ρ_0 represents the initial density of the material in the stress-free state and V_{ij} denotes the velocity of the ultrasonic wave (where i,j = 1,2,3; the direction of wave propagation is indicated by the first subscript i, and the polarization direction of the wave is indicated by the second subscript j. When $i = j$, V_{ij} is the longitudinal wave velocity V_L. When $i \neq j$, V_{ij} is the shear wave velocity V_S). λ and μ are the Lamé constants. l, m, and n

are the Murnaghan constants. σ_{11} is the normal stress in direction 1. Similarly, σ_{22} and σ_{33} are the stresses in directions 2 and 3, respectively.

When the material is in a plane stress state, it is assumed that $\sigma_{33} = 0$, and σ_{11} and σ_{22} are not zero. This condition reflects a scenario where stress is applied in two dimensions (directions 1 and 2), with no stress in the third dimension. For shear waves, the change in wave velocity caused by stress is relatively small. Therefore, it can be assumed that [28]:

$$V_{12} \cong V_{13} \cong V_{S0} \text{ but } V_{12} - V_{13} \neq 0 \tag{9}$$

where V_{S0} is the initial wave velocity of transverse waves without initial stress. According to Equation (9), Equation (8) can be simplified into two equations that are used to represent the relationship between transverse and longitudinal waves and stress.

$$\frac{(V_{12} - V_{13})}{V_{S0}} = \frac{n + 4\mu}{4\mu^2}(\sigma_{22} - \sigma_{11}) = K_S(\sigma_{22} - \sigma_{11}) \tag{10}$$

$$\frac{V_{11} - V_{L0}}{V_{L0}} = \frac{\mu l - \lambda(m + \lambda + 2\mu)}{\mu(3\lambda + 2\mu)(\lambda + 2\mu)}(\sigma_{22} + \sigma_{11}) = K_L(\sigma_{22} + \sigma_{11}) \tag{11}$$

where K_S is the acoustic elastic coefficient of the transverse wave, and K_L is the acoustic elastic coefficient of the longitudinal wave.

The propagation of ultrasonic surface waves can be considered a composite of longitudinal and transverse motions. The vibration displacement of the particle in these waves aligns with the propagation characteristics of the transverse waves. Therefore, the acoustoelastic coefficients of ultrasonic surface waves can be equated to those of the transverse waves. Under uniaxial stress, the velocity of the surface waves parallel to the stress direction is more sensitive to stress changes. The stress in the perpendicular direction can be considered negligible. The values of $\sigma_{22} = \sigma$ and $\sigma_{11} = 0$ can be set, and the relationship between the Rayleigh wave velocity and stress is then expressed as shown in Equation (12) [29].

$$\frac{V_R - V_{R0}}{V_{R0}} = K_R\sigma = K_S\sigma = \frac{n + 4\mu}{8\mu^2}\sigma \tag{12}$$

where V_{R0} represents the velocity of the ultrasonic surface waves under the stress-free state, V_R is the velocity of ultrasonic surface waves when stress is present, and K_R is the acoustoelastic coefficient for the ultrasonic surface waves. The absolute stress in the steel structure under the current conditions can be determined using Equation (12) according to the acoustoelastic coefficient and the velocities of the ultrasonic surface waves in both the stress-free and stressed states, which are measured through experimentation.

3. Finite Element Modeling

The FE analysis of laser ultrasonics is a complex problem involving thermo-mechanical coupling. Based on the fundamental theory of laser ultrasonics, the laser energy absorbed by the material creates a transient, non-uniform temperature field through thermal conduction effects around the area of laser interaction. Local thermal expansion under the action of a non-uniform temperature field will produce thermal stress which, in turn, excites the ultrasonic waves. The heat conduction is treated as the essential mechanism for laser-induced ultrasonic excitation in the FE model. Based on the principles of heat conduction and thermoelastic coupling, the process of stress measurement through laser-induced ultrasonic can be simulated using the software, COMSOL Multiphysics version 6.1.

3.1. Setting of Model Parameters

In the FE model, the material was modeled as isotropic Q235 steel, characterized by dimensions of 30 mm in length and 10 mm in width. The thermal and mechanical properties pertinent to this steel type are systematically outlined in Table 1. To streamline the computational process, the process of laser excitation of ultrasound on the surface

of a solid was equivalent to a two-dimensional plane strain model. This approximation facilitated a more manageable analysis while capturing the essential aspects of the laser-material interaction. In the model, the laser pulse was directed to impinge upon the central area of the surface of the material. The configuration and details of this FE model are depicted in Figure 4.

Table 1. Physical parameters of Q235.

Density/(kg/m^3)	Elastic Modulus/Pa	Poisson's Ratio	Thermal Expansion Coefficient/(1/K)	Thermal Conductivity/(W/(m·K))	Heat Capacity at Constant Pressure/(J/(kg·K))
7850	2.06 × 1011	0.25	0.000012	52.34	502

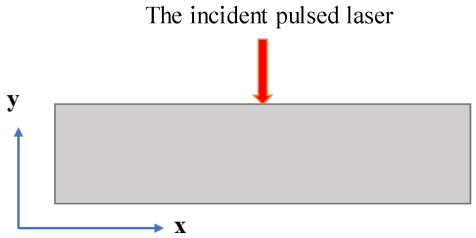

Figure 4. FE model.

The incident laser was executed as a boundary load in the FE model. This load adheres to a Gaussian distribution, integral to the formulation of the laser ultrasonic thermo-mechanical coupling model. The thermal source distribution function of the laser with Gaussian distribution in time and space is as follows [30]:

$$Q(I_0, r, z, t) = I_0 A(T) f(r) g(t) \tag{13}$$

In the equation, I_0 represents the energy density of the incident pulsed laser, measured in watts per square meter (W/m^2), and $A(T)$ denotes the absorptivity of the surface of the material to the laser. For simplification in calculations, it was assumed that the pulsed laser energy was entirely absorbed by the material, hence $A(T) = 1$. $f(x)$ is the Gaussian function describing the spatial distribution of the laser, while $g(t)$ is the Gaussian function that characterizes the temporal distribution of the laser.

In the FE model depicted in Figure 5, the pulsed laser was effectively represented by a Gaussian thermal source. The upper boundary of the model incorporated a heat flux equation that corresponded to this defined thermal source. For the analysis of the temperature field, the baseline temperature of the model was established at ambient room temperature. The boundaries of the metal material that were not subjected to laser irradiation, specifically the lower and lateral surfaces, were characterized as adiabatic, preventing heat transfer through these surfaces.

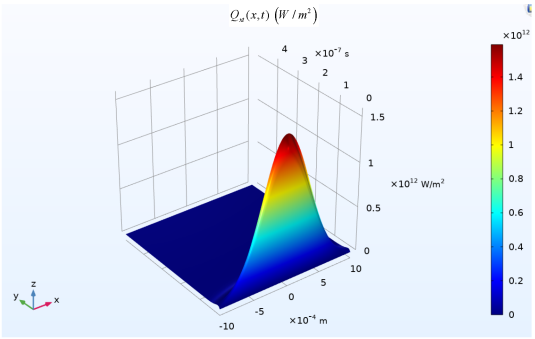

Figure 5. The Gaussian heat source.

The initial displacement and initial stress of the model were both set to zero. The upper surface of the model, directly exposed to the laser, was designated with a free boundary condition. To mitigate the influence of the reflected waves, the model incorporated low-reflection boundary conditions on the three surfaces not directly exposed to the laser irradiation. External stress or pre-stress and strain were applied to the linear elastic material within the model, serving as the external load of the model. Finally, the multi physics coupling of solid heat transfer and solid mechanics was carried out to obtain the acoustic parameters of the laser-induced ultrasound under different stresses.

Transient research was used in this study. For the solution of the transient models, their accuracy was limited by the resolution of the grid in space for waves and the resolution of the time step for temporal changes [31]. Depending on the actual needs of the model, there were different standards for dividing the grid size. In this study, the grid size L was controlled to be less than one-quarter of the ultrasonic wavelength λ [32].

Based on the relationship between ultrasonic wave speed, wavelength, and frequency, the wavelength can be determined through the ultrasonic speed and frequency. After expressing the pulsed laser using a Gaussian function, the maximum frequency of the ultrasonic wave excited by the laser was represented by a specific formula: Equation (14) [33]. By substituting C = λf into Equation (14), the minimum wavelength of the surface acoustic wave excited by the laser was obtained.

$$f_{\max} = \frac{\sqrt{2}C_R}{\pi r_0} \tag{14}$$

$$\lambda_{\min} = \frac{\pi r_0}{\sqrt{2}} \tag{15}$$

In the equation, r_0 represents the radius of the laser spot and C_R is the wave speed of the surface acoustic wave, which can be calculated using the material parameters according to Equation (16) [34]:

$$C_R = \frac{0.87 + 1.12\nu}{1 + \nu}\sqrt{\frac{\hat{E}}{2\rho(1+\nu)}} \tag{16}$$

where $\hat{E}$ represents the elastic modulus of the material, ρ is the density of the material, and ν is the Poisson's ratio of the material. In the FE model, the radius of the laser spot, r_0 was set to 0.5 mm. It was found that the minimum wavelength of the surface wave excited by the laser on the material surface was approximately 1.11 mm, using the calculation. To ensure the accuracy and reliability of the FE calculation, the grid width needed to be less than 0.28 mm. The mesh types and quantities are shown in Table 2.

Table 2. The sizes and quantity of mesh.

Finite Element Type	Quantity in Model	Mesh Size(mm)
Quad4	18,750	0.25
Tri3	9979	0.25

In the FE analysis of the laser-generated ultrasound, the time resolution needed to be sufficiently fine to ensure the reliability of the FE calculation results. Therefore, the time step, Δt should be minimized [35].

$$\Delta t = \frac{1}{180 f_{\max}} \tag{17}$$

Based on Equations (14), (16) and (17), the time step Δt can be calculated as approximately 2.67 ns. Considering the time resolution and the complexity of the computation,

the time step Δt was set to 1 ns in the FE analysis and the total time duration was set to 10,000 ns.

3.2. Analysis of Finite Element Results

Upon the incidence of the pulsed laser on the material surface, a transient temperature field was generated, subsequently exciting the production of the ultrasonic waves. First, the temperature field of the model in a stress-free state was analyzed. The temperature distribution across the entire field is shown in Figure 6, which represents the temperature field when the temperature at the laser irradiation center reached its highest, at t = 70 ns. In the figure, it can be observed that the pulse laser irradiation to the material surface caused a temperature rise only in a very small area around the laser irradiation center; the temperature of the rest of the material remained unchanged. In Figure 6, it is shown that the transient temperature field produced after laser irradiation was limited in scope, with instantaneous temperature rises occurring only within a very small area near the irradiation center; this area was only in the micron (μm) scale. Beyond this range, the change in the material surface temperature was minimal or almost non-existent. It was precisely the temperature difference between the transient temperature field and the steady temperature field that caused thermal expansion on the material surface, thereby forming the ultrasonic waves. In addition, it should be noted that the characteristics of materials under high stress change as the stress level increases, which has a certain impact on the generation of ultrasonic waves. Figure 7 shows the distribution of the full-field waveform at a particular moment. From the figure, it is evident that the incidence of the pulsed laser on the material surface excites longitudinal, transverse, and surface waves, each propagating at their respective ultrasonic wave velocities. In this study, the surface waves for stress detection were employed and the acoustic characteristics of the surface waves were analyzed.

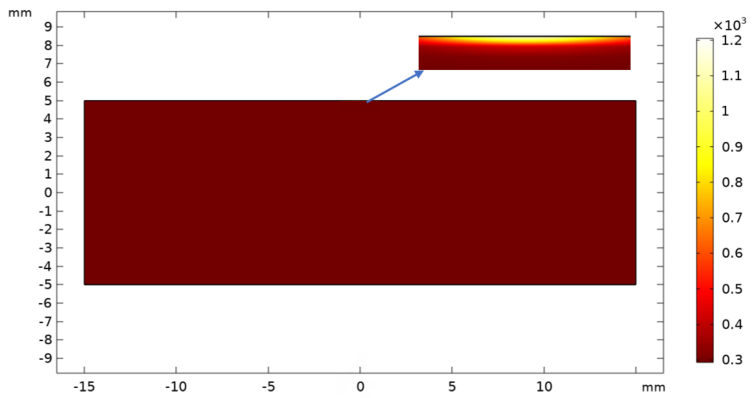

Figure 6. The temperature distribution of the whole field when t is 70 ns.

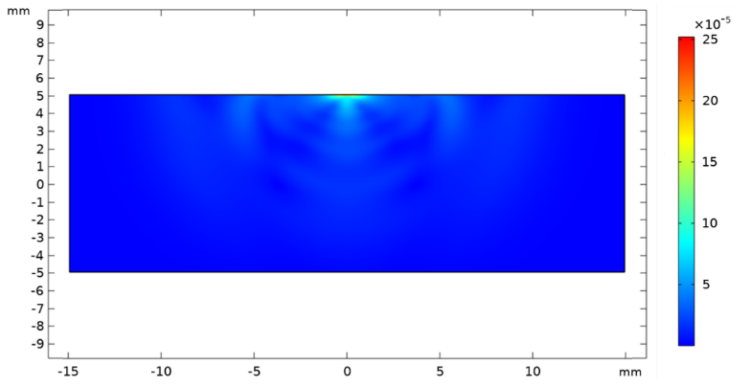

Figure 7. The waveform distribution of the entire field.

In the FE model, the signal reception points were designated at locations 2 mm, 3 mm, 4 mm, and 5 mm to the right of the laser irradiation center on the upper surface. The time-domain waveforms of the ultrasonic waves received at these points are shown in Figure 8. As observed in Figure 8, the pulsed laser incident on the material surface generates ultrasonic waves, which propagate outward in all directions at the time $t = 0$. There were similar variation characteristics for waveforms of signals at the different reception points. As the propagation distance of the ultrasonic waves increased, the amplitude of the time-domain waveforms gradually attenuated, and the wave packet widened. There were delays for the time-domain signals of the ultrasonic surface waves. Additionally, it was indicated that the flight time of the ultrasonic waves also increased progressively, consistent with the propagation characteristics of the surface waves. When the propagation distances of the ultrasonic waves were 2 mm, 3 mm, 4 mm, and 5 mm, the corresponding flight times of the ultrasonic waves were 0.7065 μs, 1.0300 μs, 1.4295 μs, and 1.8295 μs, respectively. The velocity of the ultrasonic waves was determined by linearly fitting the different propagation distances and corresponding flight times at the four signal reception points. The calculated velocity of the ultrasonic waves was 2647.06 m/s, which is close to the general propagation speed of ultrasonic waves in metals. Through the analysis of the propagation characteristics and velocity of the ultrasonic waveforms, this study identified the ultrasonic waves extracted from the upper surface of the model, at a distance to the right of the laser irradiation center, as ultrasonic surface waves. These were used in the subsequent analysis of the correlation between wave speed and stress.

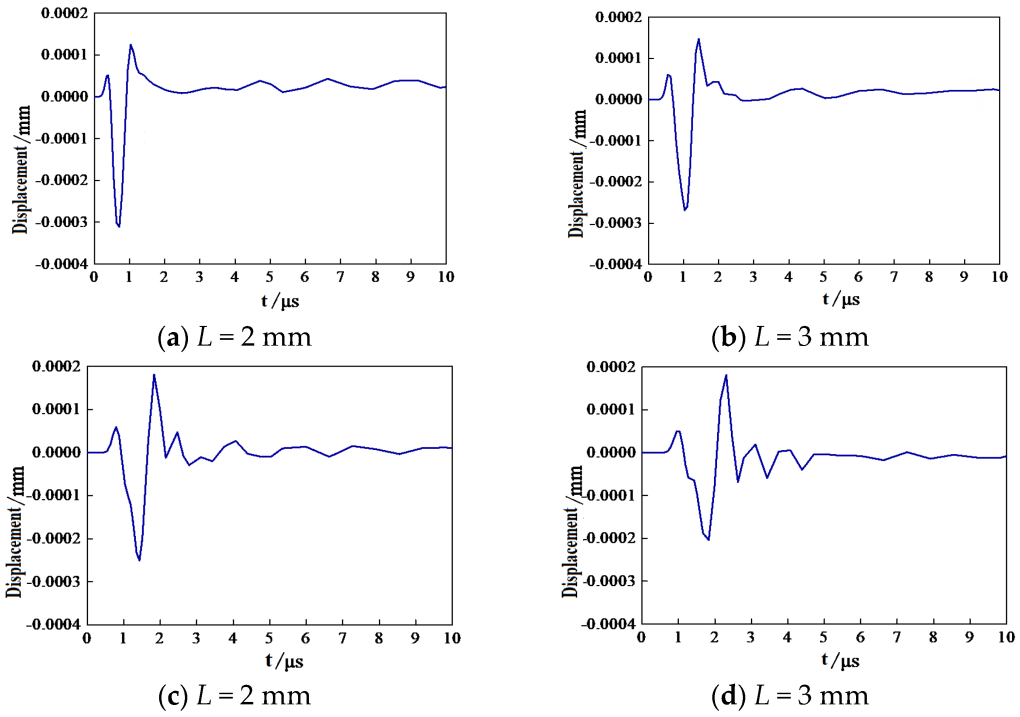

Figure 8. Ultrasonic time-domain signal at different locations.

The model was subjected to stress levels ranging from 20 MPa to 200 MPa, and the time-domain signals of the ultrasonic waves on the surface of the material under different stress levels were measured. To enhance the time resolution, the interpolation method from the multi-rate sampling technique was employed. Based on the distance between each reception point and the laser excitation point, as well as the flight time of the ultrasonic waves, the average ultrasonic wave velocity under various stress levels was determined using the method of differences. The relative wave velocity was defined as $(V - V_0)/V_0$, which can be represented as $\Delta V/V_0$. The relationship between the relative velocity of ultrasonic waves and stress is shown in Figure 9. The observation of the variation trend

of relative wave velocity with stress in Figure 9 revealed that the relative wave velocity gradually decreased with the increase of stress. This trend was consistent with the theory mentioned in the literature [36], which states that stress causes a reduction in wave velocity. Furthermore, there exists an approximately linear relationship between relative wave velocity and stress, aligning with the predictions of acoustoelastic theory. Therefore, the ultrasonic surface waves generated by pulsed laser excitation can be effectively used to measure the absolute stress on metal surfaces.

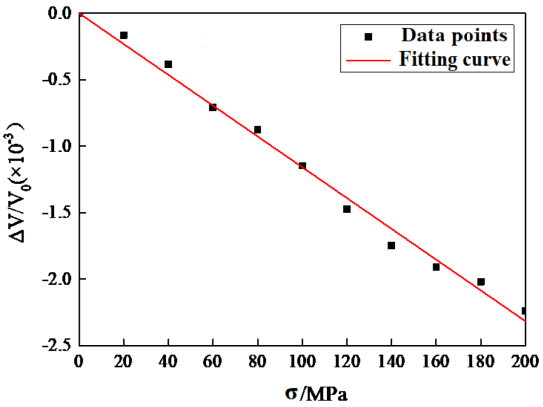

Figure 9. Relationship between the relative wave velocity of ultrasound and stress.

4. Experimental Details

4.1. Specimens Preparation

To align with the practical engineering scenarios, Q235 steel, which is a material commonly used in engineering projects, was selected as the test material in this experiment. The dimensions of the test specimens were 60 mm × 60 mm × 60 mm, and there were a total of nine specimens, as shown in Figure 10. Since the experiment involved the uniaxial compression of cubic Q235 steel specimens, and the laser excitation point and ultrasonic signal reception point were located on the same side of the specimen, it was necessary to ascertain whether the stress at the surface measurement points of the specimen was equivalent to the axially applied stress. A three-dimensional cubic model, identical in size to the test specimens, was established using the software. This model simulated the uniaxial compression process based on the loading method of the pressure testing machine. Constraints were added to the upper surface of the specimen. The stress variation on one side of the specimen is depicted in Figure 11, when a stress of 100 MPa was applied to the bottom surface. As observed in Figure 11, the stress increased near the constraints when the top surface of the specimen was constrained and the bottom surface was subjected to stress loading. However, the rest of the side surface of the specimen still experienced the magnitude of the uniaxial stress. Therefore, this experiment ensured consistency between the applied stress and the actual measured stress.

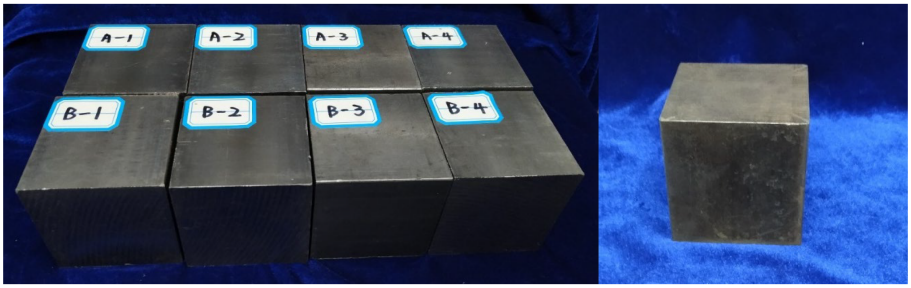

Figure 10. Q235 steel specimens.

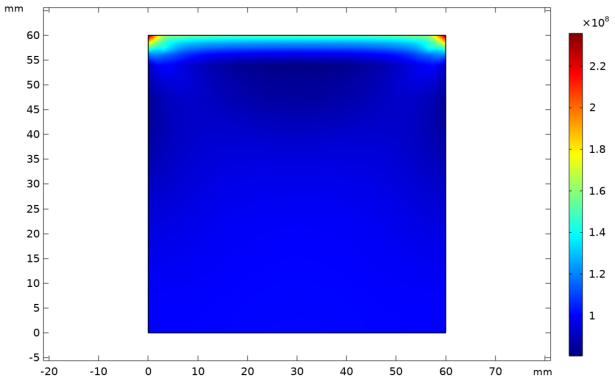

Figure 11. The distribution of stress on the side surface under uniaxial stress.

4.2. Experiment Device and Detection Scheme

To facilitate the laser ultrasonic detection of stress in steel structures, an experimental laser ultrasonic system was established, as shown in Figure 12. The experimental system comprised both laser excitation and reception devices, as well as a loading apparatus. The system included a 3D scanning platform with a displacement accuracy of 1 mm, an Nd:YAG pulsed laser with a wavelength of 1064 nm and a repetition rate of 10 Hz, a total reflection mirror, a lens, an interferometric pickup (vibrometer) with a frequency bandwidth of DC~24 MHz and a displacement resolution of 0.1 pm, an oscilloscope, a PC terminal that was used to control the sampling frequency and sampling direction parameters, and a 300-ton fully automatic pressure testing machine. Since the stress on the side surfaces of the specimen was the same, one side was chosen to perform the stress detection. Both the laser excitation device and the ultrasonic wave receiver were located on the same side of the specimen.

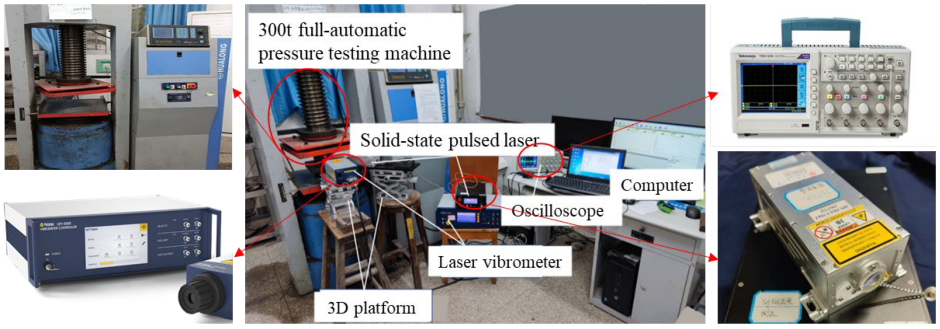

Figure 12. The laser ultrasonic testing system.

The nine Q235 steel specimens were divided into three groups for measurement, as shown in Table 2. To enhance the signal-to-noise ratio of the received ultrasonic signals, the surface of the material was polished, and aluminum foil with a thickness of about 1 mm was adhered at the signal reception points to amplify the signal strength. All tests were conducted at room temperature, which is approximately 20 °C. Group 1 was used to measure the velocity of the ultrasonic surface waves under stress-free conditions. The signal collection points were located 10 mm from the left edge of the specimen; the upper and lower edges were 30 mm each. The laser excitation points were located at different positions to the right of the collection points, with a 5 mm interval between each point. Scanning from left to right according to the path shown in Figure 13 allowed for the collection of time-domain signals of the ultrasonic waves at different positions. Groups 2 and 3 were used for the loading tests. Taking specimen A1 as an example, it was placed between the upper and lower platens of the pressure testing machine. The collection point was fixed at the center of the side surface of the specimen, and the laser excitation point was located below the collection point. The distance between the laser excitation point and the signal

collection point was distributed as shown in Table 3. The ultrasonic wave propagation direction was aligned with the principal stress direction, as illustrated in Figure 14.

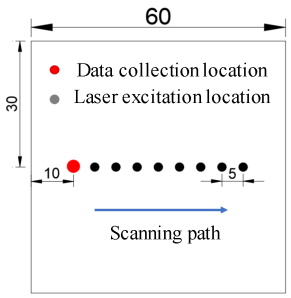

Figure 13. The scanning path of the specimen under stress-free conditions/mm.

Table 3. The situation for sample grouping.

Group	The Number of Specimens	Distance between Incentive Point and Acquisition Point *L*/mm	The Purpose
1	SD-1	5—40	Analyzing the variation of Rayleigh wave velocity under stress-free conditions
2	A1 A2 A3 A4	15 15 10 20	Detecting the variation of wave velocity with stress at the same/different positions of the test block
3	B1 B2 B3 B4	15 15 10 20	Repeating group for Group 2

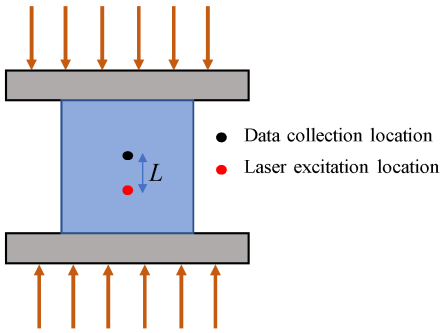

Figure 14. The scanning path of the specimen under stress conditions/mm.

After completing the ultrasonic wave measurements under stress-free conditions, the test machine was controlled to apply the load to the specimens according to a pre-set program, with a loading increment of 20 MPa, and continuing up to a maximum of 200 MPa. At each stress level during loading, the testing machine was stabilized in the load-holding state and the ultrasonic wave signals received by the oscilloscope were saved. Due to the vibrations of the pressure testing machine, the specimens placed on it would also vibrate. This caused random changes in the relative position between the laser vibrometer and the specimen, and led to a deviation of the signal collection point from its original position. Therefore, the signals at the measurement points were collected multiple times and averaged to reduce the errors caused by the operational characteristics of the testing machine.

4.3. Analysis and Discussion

During the experimental process, although the oscilloscope sampling filtered out some noise, further filtering of the specific frequency bands from the signal was still required to ensure accurate analysis and processing of the ultrasonic wave signals. For the ultrasonic signals, there is often more information for low-frequency components, whereas high-frequency components are typically associated with noise. In this study, the Sym8 wavelet was used to decompose the experimentally obtained ultrasonic wave signals. The decomposition was performed over five levels, and a soft thresholding function [37] was chosen to achieve this purpose. A comparison of the ultrasonic surface wave signals before and after wavelet denoising is illustrated in Figure 15.

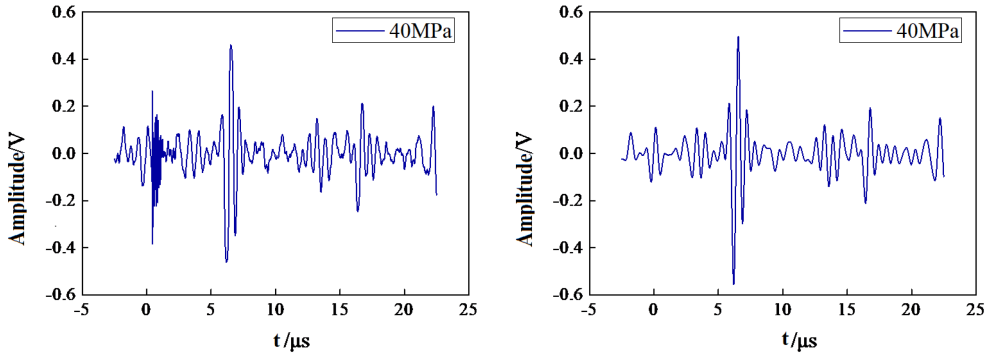

Figure 15. Ultrasonic time-domain signal for B1. (**a**) Ultrasonic time—domain signal before wavelet denoising; (**b**) Ultrasonic time-domain signal after wavelet denoising.

Upon comparing the time-domain signals before and after denoising, it was observed that the noise components within the signal were effectively removed, leading to an enhanced signal-to-noise ratio and a smoother time-domain curve. Additionally, the denoised ultrasonic signals were further processed using a cubic spline interpolation method to improve the resolution of the time difference measurements. A comparison of the ultrasonic surface wave signals before and after interpolation is depicted in Figure 16. While the overall trend of the time-domain signal curve remained unchanged, the resolution was enhanced and the precision in extracting time differences was improved post interpolation. The waveforms of the ultrasonic signals received at various stress levels were similar, with a consistent frequency and other characteristics, and differed only in the arrival time of the ultrasonic waves. The velocity of the ultrasonic surface waves was determined by reading the time delay in the ultrasonic wave time-domain waveforms and combining it with the distance over which the ultrasonic wave was propagated.

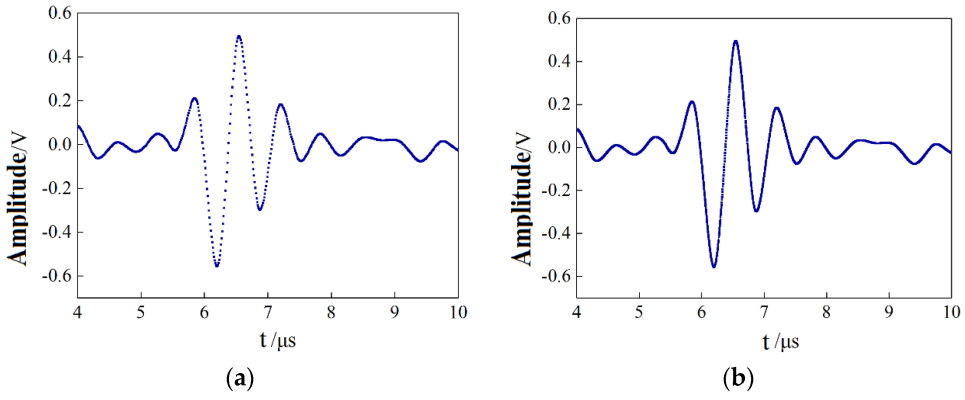

Figure 16. Ultrasonic time-domain signal for B1. (**a**) Ultrasonic time-domain signal before interpolation (**b**) Ultrasonic time-domain signal after interpolation.

In the context of the Q235 steel structural specimens subjected to uniaxial loading, a subtle expansion occurs on the side surfaces of the specimens due to compression. This phenomenon leads to an extended propagation path for the surface waves, as depicted in Figure 17. While the magnitude of the surface expansion during the elastic phase of the specimen was relatively minor, the influence of the distance alterations on the variations in wave velocity was notably significant. Consequently, it became imperative to account for the effects of surface expansion of the specimen when conducting laser ultrasonic testing. This consideration was crucial for ensuring the accuracy and reliability of the ultrasonic measurements, particularly in stress analysis and material characterization applications.

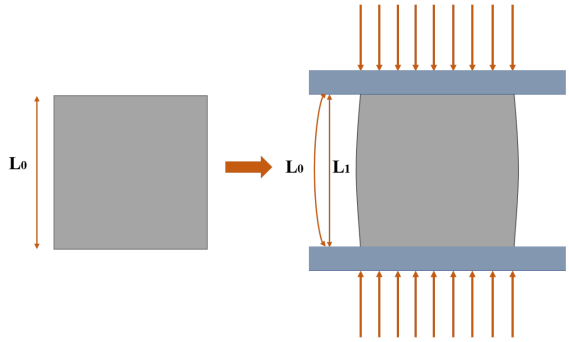

Figure 17. The surface changes of the specimen during the loading process.

For specimens subjected to uniaxial compression, the acoustoelastic coefficient is a key factor in calculating stress. The acoustoelastic coefficient can be expressed as follows:

$$C_R = \frac{v_R - v_{R0}}{v_{R0}\sigma} \tag{18}$$

The calculated velocities of the ultrasonic surface waves under both stress-free and stress-loaded conditions can be represented as follows:

$$v_{R0} = \frac{\mathrm{L}}{t_0}, v_R = \frac{\mathrm{L}_\Delta}{t_\sigma} \tag{19}$$

In the equation, L denotes the theoretical distance over which the ultrasonic wave propagates. $\mathrm{L}_\triangle$ denotes the actual distance over which the ultrasonic wave propagates. The variables t_0 and t_σ represent the travel times of the ultrasonic wave for this theoretical propagation distance under two different conditions: t_0 is the travel time when there is no applied stress, and t_σ is the travel time when the specimen is subjected to a stress of σ. Taking into account the surface expansion of the specimen leads to an increase in the propagation distance (L), as used in the computation of the Rayleigh wave velocity (V_R) in Equation (19). Under identical stress and wave travel time conditions, this adjustment resulted in a higher calculated wave velocity. Subsequently, as per the formulation in Equation (18), there is a consequential increase in the acoustoelastic coefficient so that there are some errors in the calculation of the stress.

To eliminate the impact of the lateral surface expansion of the specimen, the wave velocity was calculated using the actual propagation distance $\mathrm{L}_\triangle$ of the ultrasonic wave after determining the time delay, as illustrated in Figure 18. During the uniaxial compression process, the expansion curve of the specimen was approximately parabolic. A Cartesian coordinate system was established with the midpoint of the parabola as the origin. The arc length direction was set as the x-axis and the direction perpendicular to the arc length was set as the y-axis. The origin of the coordinate system was spatially parallel to the signal reception point and can be considered as the signal reception point itself.

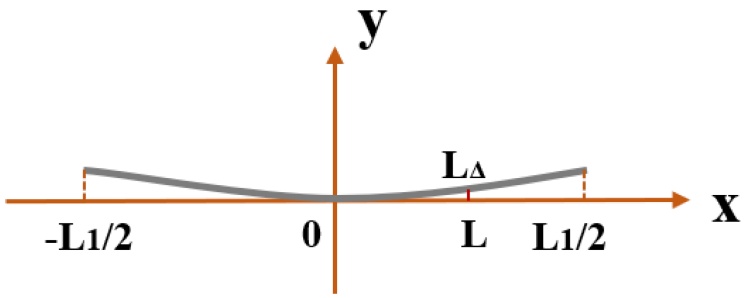

Figure 18. Changes of specimen during loading process.

The original side length of the specimen was L_0. When compressed and expanded, the length of the side itself remained unchanged, and it can be assumed that the arc length of the expanded parabola was L_0. At this time, the distance between the upper and lower platens of the testing machine was L_1. The stress applied to the specimen by the testing machine was achieved by moving the lower platform upwards, so that L_1 is equal to $L_0 - \Delta x$. Δx is the displacement of platform of the testing machine. It can be obtained from the control interface of the testing machine. As shown in Figure 18, the horizontal coordinates of the two ends of the parabola were $\pm L_1/2$. L is the theoretical propagation distance of the ultrasonic wave, and $L_\triangle$ is the actual propagation distance of the ultrasonic wave. It is necessary to calculate the arc length of the parabola from the horizontal coordinate zero to L. The solution expression is as follows:

$$L_\Delta = \int_0^L \sqrt{1 + \frac{1}{p^2} x^2} dx \tag{20}$$

where p can be obtained through the parabolic equation. The calculation results for the actual propagation distance of the surface waves on the specimen are shown in Tables 4 and 5. From these tables, it is evident that the farther the distance between the laser excitation point and the signal reception point, the greater the change in the actual propagation distance of the surface waves during compression expansion. For a theoretical propagation distance of 20 mm, a stress of 200 MPa results in a change of approximately 0.1 to 0.2 mm in the propagation distance, leading to a change of approximately 1% in the ultrasonic wave velocity. Since the acoustoelastic effect is a weak effect, it is essential to consider the changes in wave velocity caused by variations in the propagation distance. Subsequently, calculations of ultrasonic wave velocity were performed using the expanded propagation distance. The relationship curves between the relative wave velocity and stress for specimens A1 and B1, from the stress-free state to bearing 200 MPa, are shown in Figure 19.

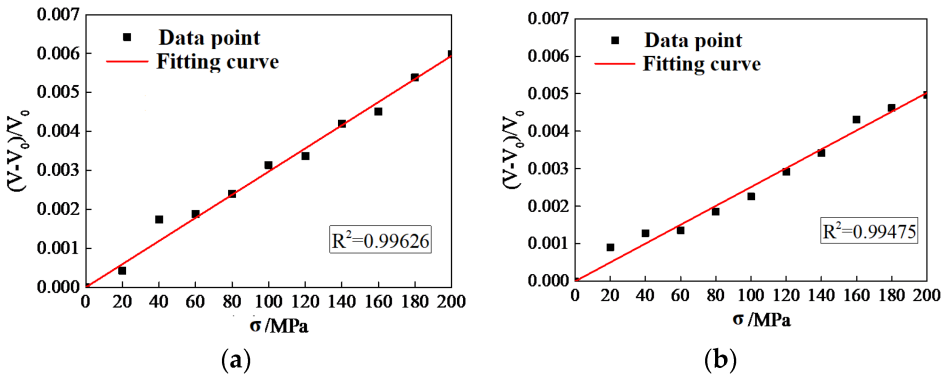

Figure 19. The relationship between the relative wave velocity and stress. (**a**) The relationship for A1 (**b**) The relationship for B1.

Table 4. The actual propagation distance of the surface waves for Group 2.

A1		A2		A3		A4	
σ/MPa	**Actual Propagation Distance/mm**	**σ/MPa**	**Actual Propagation Distance/mm**	**σ/MPa**	**Actual Propagation Distance/mm**	**σ/MPa**	**Actual Propagation Distance/mm**
0	15	0	15	0	10	0	20
20	15.0166	20	15.0096	20	10.0047	20	20.0136
40	15.0248	40	15.0182	40	10.007	40	20.0285
60	15.0322	60	15.0251	60	10.0089	60	20.0428
80	15.039	80	15.0317	80	10.0108	80	20.0566
100	15.0453	100	15.0378	100	10.0126	100	20.0691
120	15.0514	120	15.0437	120	10.0143	120	20.0809
140	15.0577	140	15.0496	140	10.016	140	20.0935
160	15.0642	160	15.0555	160	10.0177	160	20.1061
180	15.0706	180	15.0612	180	10.0194	180	20.1187
200	15.077	200	15.0669	200	10.021	200	20.1312

Table 5. The actual propagation distance of the surface waves for Group 3.

B1		B2		B3		B4	
σ/MPa	**Actual Propagation Distance/mm**	**σ/MPa**	**Actual Propagation Distance/mm**	**σ/MPa**	**Actual Propagation Distance/mm**	**σ/MPa**	**Actual Propagation Distance/mm**
0	15	0	15	0	10	0	20
20	15.0095	20	15.0156	20	10.0033	20	20.0469
40	15.0205	40	15.0331	40	10.0072	40	20.0857
60	15.028	60	15.0478	60	10.0098	60	20.1176
80	15.0342	80	15.0588	80	10.012	80	20.1445
100	15.0398	100	15.0676	100	10.0141	100	20.1655
120	15.045	120	15.0751	120	10.016	120	20.1835
140	15.0499	140	15.086	140	10.018	140	20.2004
160	15.0548	160	15.0886	160	10.0198	160	20.2165
180	15.0595	180	15.0952	180	10.0216	180	20.2319
200	15.0641	200	15.1015	200	10.0359	200	20.2475

Figure 19 presents the relationship between the relative wave speed and stress. From Figure 19, it is indicated that there is an approximate linear relationship between relative wave speed and stress, consistent with the simulation analysis. To clearly characterize the linear relationship between the relative wave speed and stress, the curve has been linearly fitted. The fitting goodness R^2 was above 0.99, indicating a strong linear relationship between the relative wave velocity and stress, which is in line with the requirements of the acoustoelastic equation. In the process of stress solving, the acoustoelastic coefficient C_R is a key parameter for the solution. Based on Equation (18), the acoustoelastic coefficient can be obtained through the linear relationship between the ultrasonic relative wave speed and stress. The slope of the fitted curve is the acoustoelastic coefficient. The obtained acoustoelastic coefficients for the various specimens fluctuated between 2.51×10^{-5} and 3.21×10^{-5}, which was minimal variance among different specimens. Therefore, the acoustoelastic coefficient of specimen A1, 2.97×10^{-5}, was chosen as the optimal coefficient for calculating the absolute stress of the specimens.

Based on the acoustoelastic coefficient obtained, the absolute stress for specimens was calculated. The results of the stress measurement and their theoretical values are shown in Figures 20–22. Due to the surface roughness of the steel specimens used in the experiment and the fact that the material uniformity cannot be guaranteed to be completely consistent, the acoustoelastic coefficients of the different specimens are different. In addition, the measurement results are also influenced not only by material characteristics but also by the

stress level and the distance of ultrasonic wave propagation. Therefore, there will be errors for the calculated absolute stress. Figures 20–22 show the results of stress detection at the different ultrasonic propagation distances. From the figures, it can be observed that the absolute error between the measured stress and the theoretical stress of the specimens was the largest when the stress level was low. When the ultrasonic propagation distance was 15 mm, the maximum absolute errors between the measured stress and the theoretical stress of specimens A1, B1, A2, and B2 were 18.48 MPa, 16.07 MPa, 21.92 MPa, and 15.35 MPa, respectively, with average errors of 5.18 MPa, 7.46 MPa, 11.45 MPa, and 7.89 MPa. When the ultrasonic propagation distance was 10 mm, the maximum absolute errors between the measured stress and the theoretical stress of specimens A3 and B3 were 21.92 MPa and 33.52 MPa, respectively, with average errors of 11.45 MPa and 20.66 MPa. When the ultrasonic propagation distance was 20 mm, the maximum absolute errors between the measured stress and the theoretical stress of specimens A4 and B4 were 18.46 MPa and 15.38 MPa, respectively, with average errors of 7.03 MPa and 8.12 MPa. Overall, compared with the other specimens, the stress measurement error was the largest when the ultrasonic propagation distance was 10 mm. The main reason is that the distance between the laser excitation point, and the signal collection point was too close, causing the laser spot energy to interfere with the beam of the laser vibrometer, leading to greater data volatility. Therefore, it is necessary to ensure that the excitation point and the measurement point are sufficiently far apart when measuring the stress.

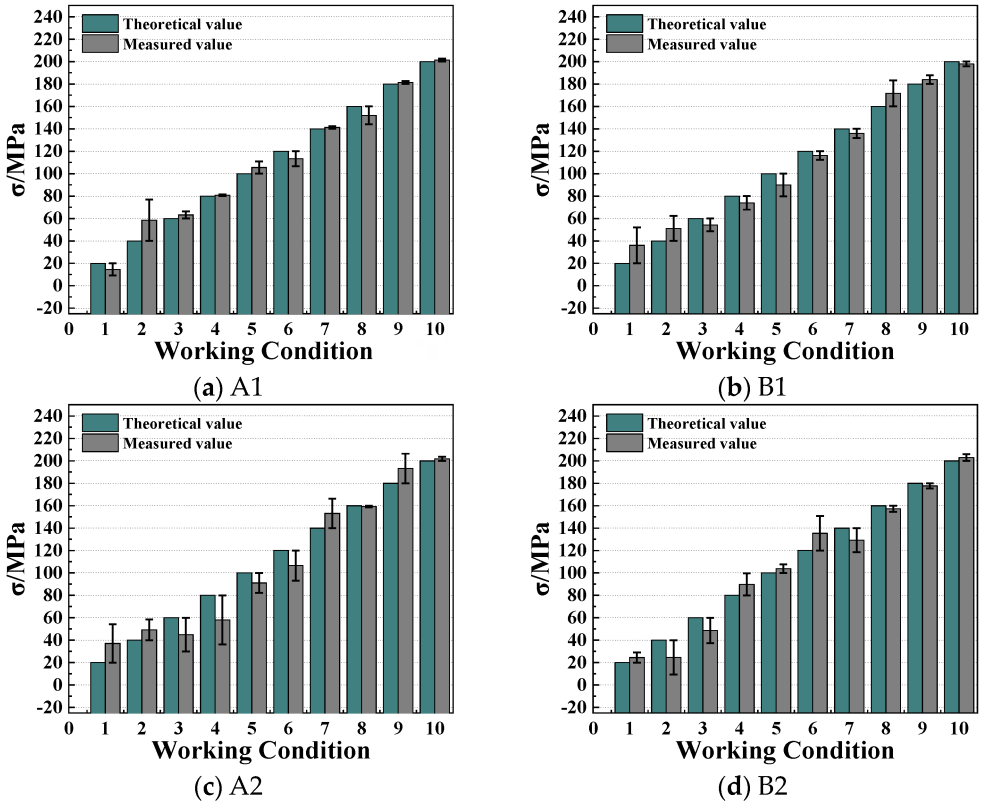

Figure 20. Stress calculation results for theoretical propagation distance at 15 mm.

Figure 23 presents the relative errors in the experimental results at different stress levels. As the stress level continued to increase, the relative error between the calculated stress and the theoretical stress of the specimens gradually decreased. When the stress of the steel component was 20 MPa, the relative error of the measurement results was the largest, with a maximum relative error of 85.3%. When the stress of the steel component was 200 Mpa, the relative error of the measurement results was the smallest, with a minimum relative error of 0.4%. In addition, it was found that the relative errors were

generally within 10% when the stress was 100 Mpa and above. Overall, the laser ultrasonic method demonstrates good reliability and accuracy in measuring the absolute stress of steel structures, especially at higher stress levels. This makes this method a viable option for engineering measurements. In practical engineering applications, if there is a need to measure the absolute stress of a steel structure, it is only necessary to calibrate the test specimens of the steel structure to obtain the acoustoelastic coefficient. The absolute stress of the steel components can be determined through the acoustoelastic formula, using the laser ultrasonic method to detect the relative velocity of the ultrasonic surface waves. This approach offers a practical and efficient solution for assessing the stress state in steel structures, which is crucial for ensuring their structural integrity and performance.

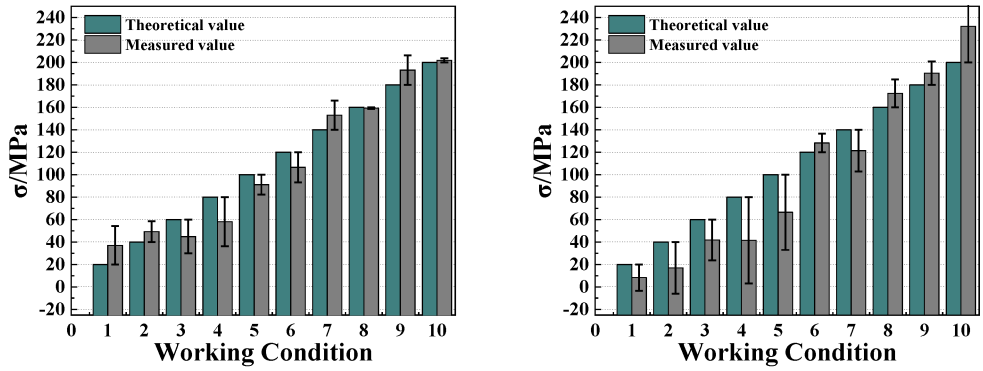

Figure 21. Stress calculation results for theoretical propagation distance at 10 mm.

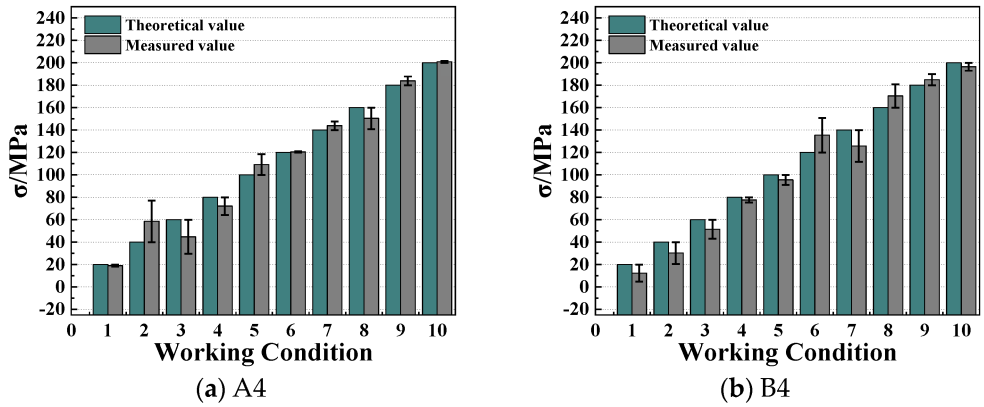

Figure 22. Stress calculation results for theoretical propagation distance at 20 mm.

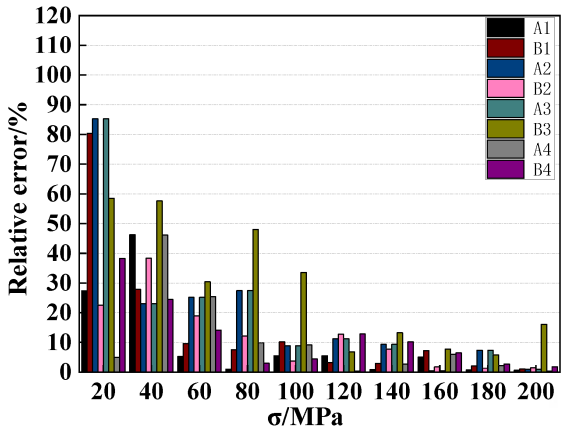

Figure 23. Relative error of stress calculation results.

5. Analysis of the Influencing Factors for Laser Ultrasonic Technology

5.1. Sensitivity of Stress Detection to Environmental Temperature

When using the laser ultrasonic method to detect the absolute stress in steel structures, changes in environmental temperature will affect the propagation of the ultrasonic waves in the following ways:

(1) Change in the propagation speed of the ultrasonic surface waves

According to the literature [34], it is known that the velocity of the surface waves in an isotropic solid under no stress is primarily related to the elastic modulus of the material, the density of the material, and Poisson's ratio, and is directly proportional to the elastic modulus. Changes in temperature generally cause changes in the elastic modulus and Poisson's ratio of steel structural materials.

According to the literature [38], the variation of the elastic modulus of several commonly used steels in engineering with temperature is usually described in detail, as shown in Figure 24. Since the change in Poisson's ratio within 100 °C is negligible, temperature mainly causes changes in the elastic modulus of the material. The increase in temperature leads to a decrease in the elastic modulus of metal materials, as shown in the Equation (21) [34].

$$E_T = E_0(1 - \eta \Delta T) \tag{21}$$

where E_T is the elastic modulus of the material when the temperature reaches, E_0 is the initial elastic modulus of the material, and η is the temperature variation coefficient of the elastic modulus of the metal. This coefficient is difficult to determine, but it is related to the metal material's linear expansion coefficient α. According to the results calculated using the experimental values in reference [39], η is approximately 25 times α. Therefore, the surface wave velocity, which is directly proportional to the elastic modulus, also decreases with the increase in temperature. The change in the velocity of ultrasonic surface waves under the influence of temperature can be expressed using the following equation:

$$V_{RT1} = V_{R0}(1 - \beta \Delta T) \tag{22}$$

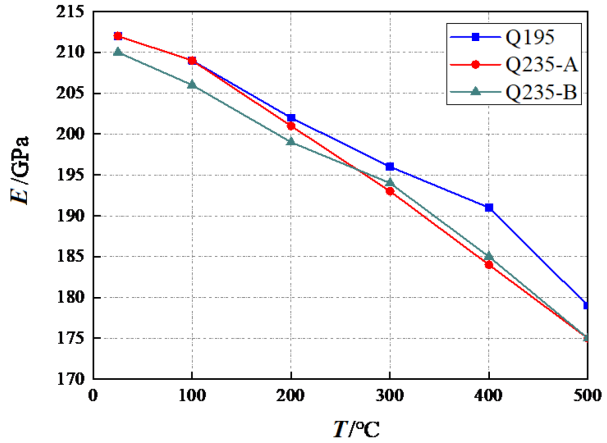

Figure 24. The elastic modulus at different temperatures.

In this equation, V_{RT1} is the wave velocity of the ultrasonic surface wave corresponding to the change in the elastic modulus when the temperature reaches T; V_{R0} is the wave velocity of the ultrasonic surface wave at the initial temperature, with no stress in the steel structure; β is the temperature coefficient of the change in the surface wave velocity with temperature, and ΔT is the change in temperature.

(2) Change in the propagation distance of the ultrasonic surface waves

Due to the thermal expansion and contraction of the materials with temperature changes, the propagation distance of ultrasonic waves is also affected. As the temperature rises, the propagation distance of the ultrasonic waves increases.

$$L_T = L_0(1 + \alpha\Delta T) \tag{23}$$

where L_0 is the initial ultrasonic wave propagation distance, L_T is the propagation distance of the ultrasonic waves at temperature T, α is the thermal expansion coefficient of the metal materials, and ΔT is the temperature change amount. The velocity of the ultrasonic surface wave after the temperature increase can be represented using the following equation:

$$V_{RT2} = \frac{L_0(1 + \alpha\Delta T)}{t_T} \tag{24}$$

In this equation, V_{RT2} is the wave velocity of the ultrasonic surface wave corresponding to the change in the elastic modulus when the temperature reaches T; t_T is the ultrasonic wave flight time when the temperature reaches T.

For metal materials, the increase in temperature leads to a decrease in the ultrasonic wave velocity, which is caused by both a decrease in the elastic modulus and an increase in the ultrasonic wave propagation distance. Therefore, the ultrasonic wave velocity when the temperature increases to T is as follows:

$$V_{RT} = V_{RT1} - (V_{R0} - V_{RT2}) \tag{25}$$

According to the literature [40], the change in the linear expansion coefficient α is relatively small compared with the change in the temperature coefficient β and can be ignored. Combining Equations (22) and (24), the change in the relative wave velocity with temperature can be expressed as follows:

$$\frac{V_{RT} - V_{R0}}{V_{R0}} = -\beta\Delta T + \frac{t_0}{t_T} - 1 \tag{26}$$

where t_0 is the flight time of the ultrasonic surface wave measured at the initial temperature. When the temperature increases, t_0 is less than t_T. From Equation (26), it can be established that the relative wave speed decreased approximately linearly with the increase in temperature.

Based on the above analysis, the effect of temperature on ultrasonic wave propagation characteristics is simulated by changing the elastic modulus. Taking 25 °C as the initial temperature, the results obtained from the model are shown in Figures 25 and 26.

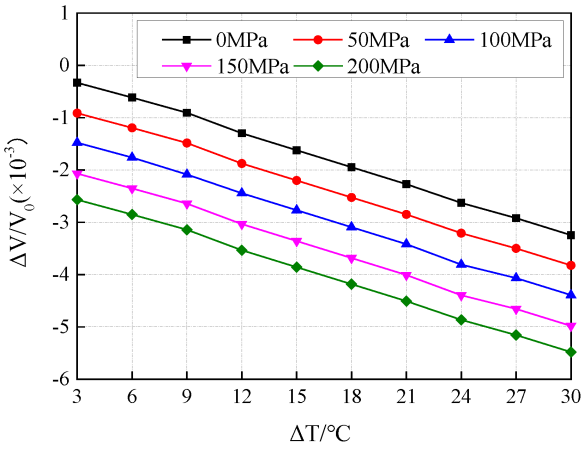

Figure 25. The variation in the relative wave velocity with temperature under different stress levels.

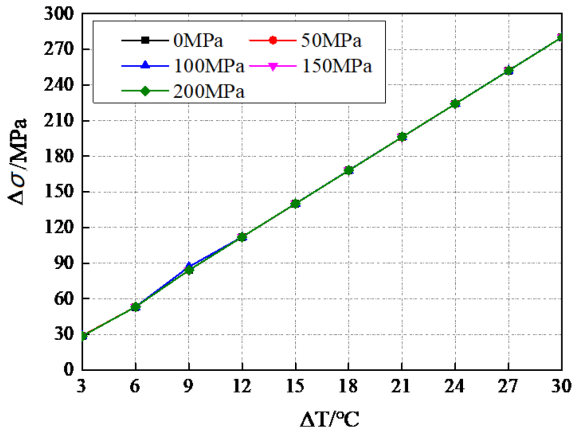

Figure 26. The variation in the stress differential with temperature under different stress levels.

In Figure 25, the relative wave speed of the ultrasonic wave decreased approximately linearly at the same stress level as the temperature increased. The change in stress affected the change in relative wave speed but did not alter the trend of change with temperature. Under the same temperature change, the higher the stress level, the lower the relative wave speed of the ultrasound. To more clearly understand the impact of ambient temperature on the stress calculation results, the deviation of calculated stress at different stress levels with temperature change is shown in Figure 26. The results indicate that an increase in temperature caused a significant error in the stress calculation. Under the same temperature change, the stress error values at various stress levels were approximately consistent. The stress deviation exceeded 270 MPa when the environmental temperature changed by 30 °C. At this time, the error far exceeded the measured value, making the stress measurement results no longer of reference value. To reduce the impact of temperature changes on stress detection, it is necessary to conduct the detection in an environment where the temperature is relatively stable.

When temperature changes are inevitable, it is necessary to propose compensation methods for the temperature variations. According to Equation (26), the temperature coefficient β is fitted based on the relationship between relative wave speed and the change in temperature. Temperature errors are compensated based on the temperature coefficient. The temperature compensation equation obtained using Figure 25 is as follows:

$$\frac{V_{RT} - V_{R0}}{V_{R0}} = -1.0816 \times 10^{-4} \Delta T + 8.4286 \times 10^{-5} \quad (27)$$

According to Equation (27), the stress calculation results after compensation are shown in Figure 27. It can be seen from Figure 27 that the stress after temperature compensation is close to those at the initial temperature, with a maximum error of 3.68 MPa. This indicates the effectiveness of the temperature compensation equation.

5.2. Sensitivity of Stress Detection to Material Surface Roughness

The surfaces of metal materials, such as steel structures, are not absolutely smooth. Scratches and other uneven undulations may exist on the surfaces of materials, which are defined as the surface roughness of the material. The inevitable random roughness of the material surface will undoubtedly affect the propagation of the surface waves when using the laser ultrasonic method to detect the absolute stress in steel structures; therefore, the measurement accuracy of stress will be affected.

To study the impact of the material surface roughness on the propagation characteristics of ultrasonic waves, it is necessary to establish a relevant model for targeted analysis. Typically, the creation of a random rough surface is performed using the Monte Carlo method. A random rough surface is composed of a superposition of harmonics with different frequencies. The height of each point on the rough surface represents the amplitude

of these superimposed harmonics. After randomly generating a two-dimensional rough surface using the Monte Carlo method, the rough surface curve was discretized into sample point data. The contour arithmetic mean deviation, *Ra*, was used to determine the degree of surface roughness and ten sets of rough surfaces with *Ra* values ranging from 0.3 μm to 3 μm were selected. The FE model is shown in Figure 28.

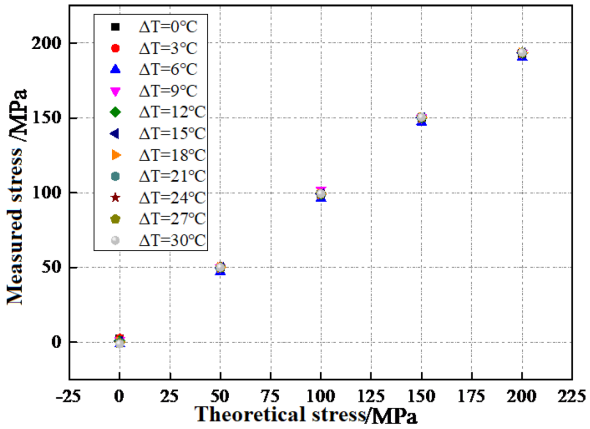

Figure 27. Measured results after temperature compensations.

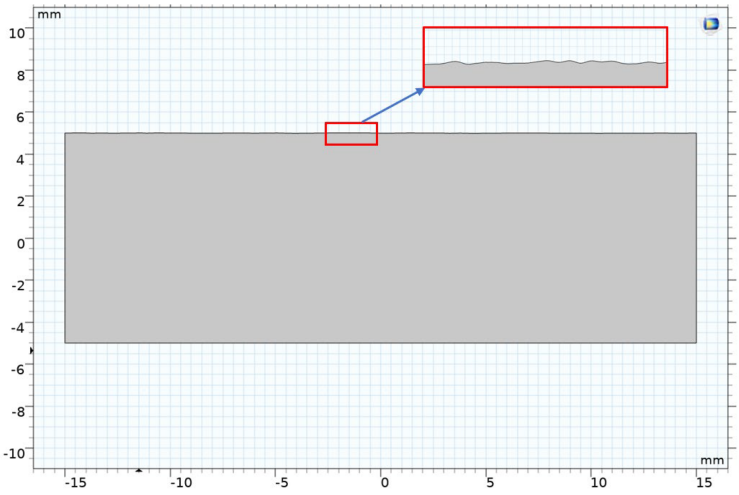

Figure 28. The FE model with a rough surface.

The curve showing the change in relative wave speed of the ultrasonic surface waves with different roughness at different stress levels is illustrated in Figure 29. From Figure 29, it can be observed that the relative wave speed decreased nonlinearly, as the roughness of the material surface increased at the same stress level. At different stress levels, the non-linear relationship between relative wave speed and material surface roughness was similar. At the same time, the deviation of calculated stress at different stress levels with changes in material roughness is represented in Figure 30. From Figure 30, it can be seen that the stress error showed a non-linear growth trend as the increase in surface roughness for the steel specimen was at the same stress level. The variation trend of stress error with changes in roughness remains essentially consistent at different stress levels. When the roughness is approximately 3 μm, the difference in stress exceeds 50 MPa. At this time, the measurement results are no longer of reference value. In summary, it is necessary to polish the surface of the test piece with fine sandpaper or a grinder before the detection, due to the impact of material surface roughness on stress detection. This will ensure the accuracy of the detection results.

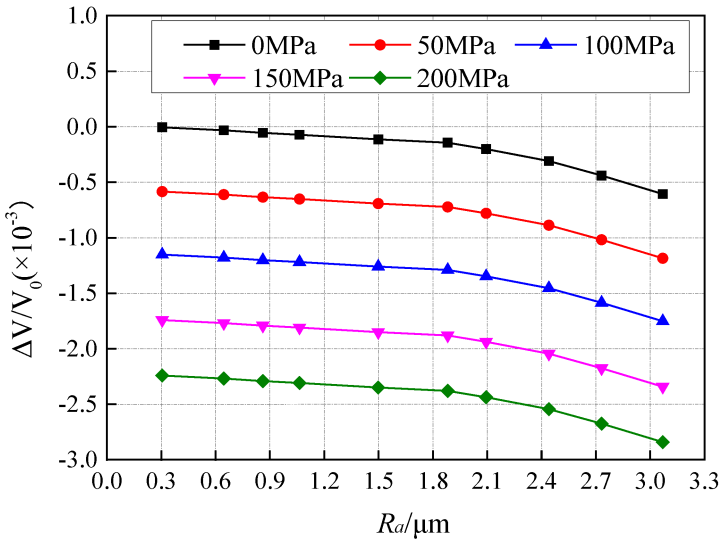

Figure 29. The variation in the relative wave velocity with *Ra* under different stress levels.

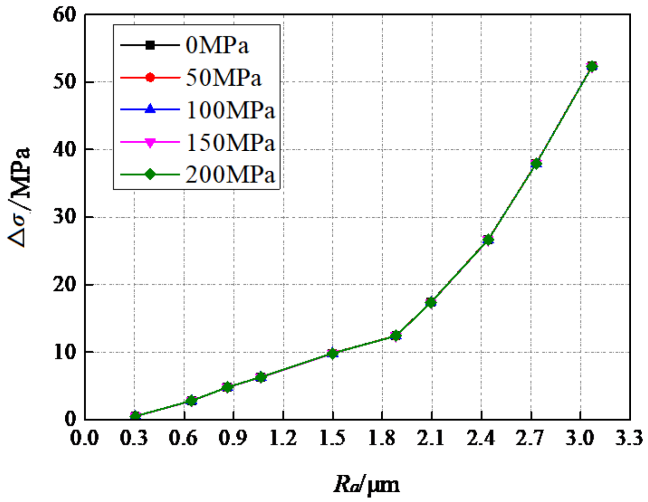

Figure 30. The variation in the stress differential with *Ra* under different stress levels.

6. Conclusions

In this work, laser ultrasonic technology was used for the measurement of absolute stress in steel structures. The velocity variation of laser-induced ultrasonic waves caused by stress variations in steel structures was analyzed based on the experiment and FE simulation. The experimental and FE results are consistent and indicate that the relative wave velocity of the ultrasonic wave is approximately linearly related to the applied stress, and that the stress can be obtained based on the linear relationship. The results confirm the feasibility of using laser ultrasonics to measure the absolute stress of steel structures.

The experimental results show that the absolute error between the measured stress and the theoretical stress of the specimens is largest when the stress level is low, and that the relative error of measured stress gradually decreased as the stress increased. When the stress experienced by the specimen was above 100 MPa, the relative error was generally within 10%. It has been proven that this technology for stress measurement has good reliability and accuracy at a high stress level.

Considering the temperature and material surface roughness as the two main influencing factors of stress detection, the sensitivity for stress detection to these factors was analyzed based on theoretical analysis and FE. The analysis results indicate that the error in stress measurement increased similarly linearly with the increase in temperature and

increased non-linearly with the increase in roughness. Consequently, error compensation methods tailored for different influencing factors were proposed, effectively enhancing the accuracy of absolute stress detection methods for steel structures.

The research on laser ultrasonic stress measurement in this paper focuses on the surface stress of specimens under uniaxial stress loading. However, steel structures in actual service are subject to complex stresses; therefore, the study of laser ultrasonic detection methods in actual steel structures is necessary. Additionally, the nonlinear geometrical effects along the members will be experimentally considered in the future.

Author Contributions: Conceptualization, Z.H.; methodology, L.L., Z.H. and H.T.; Software, Y.K.; Validation, B.L.; investigation, B.O. and B.L.; resources, Z.H.; data curation, H.T. and Y.K.; writing—original draft, H.T. and Z.H.; writing—review and editing, L.L.; supervision, L.L.; funding acquisition, L.L. All authors have read and agreed to the published version of the manuscript.

Funding: This study was supported by the National Natural Science Foundation of China (U20A20314, 52278146, 52278291), the Natural Science Fund for Distinguished Young Scholars of Chongqing (cstc2020jcyj-jqX0006), the Chongqing Natural Science Foundation of China (cstc2019jcyj-cxttX0004, cstc2020yszx-jscxX0003), and the Science and Technology Project of Guizhou Provincial Transportation Department (2020-123-017).

Data Availability Statement: The data presented in this study are available from the first and corresponding author upon request. The data are not publicly available due to the policy of the data provider.

Conflicts of Interest: Authors Hongsong Tian, Yujiang Kong, Bin Liu and Bin Ouyang were employed by the company Guizhou Bridge Construction Group Co., Ltd. The remaining authors declare that the research was conducted in the absence of any commercial or financial relationships that could be construed as a potential conflict of interest.

Abbreviations

u	the displacement component;
ε_{ij}	the component of the strain tensor;
ρ	the density of materials;
f_i	the external force applied;
T	the increase in temperature;
λ, μ	Lamé constant;
δ_{ij}	the unit tensor;
α	the coefficient of thermal expansion;
U	the displacement vector;
I	the identity tensor;
σ	the stress tensor;
n	the unit vector perpendicular to the material's surface;
V_L	the longitudinal wave velocity;
V_S	transverse wave velocity;
l, m, n	the Murnaghan constants;
K_S	the acoustic elastic coefficient of the transverse wave;
K_L	acoustic elastic coefficient of the longitudinal wave;
V_{S0}	the initial wave velocity of transverse waves without initial stress;
V_{R0}	the velocity of ultrasonic surface waves under the stress-free state;
K_R	the acoustoelastic coefficient for ultrasonic surface waves;
λ	the ultrasonic wavelength;
C_R	the wave speed of the surface acoustic wave;
$\hat{E}$	the material's elastic modulus;
ν	the material's Poisson's ratio;
r_0	the radius of the laser spot;
E_T	the elastic modulus of the material when the temperature reaches T;
E_0	the initial elastic modulus of the material;

η	the temperature variation coefficient of the metal's elastic modulus;
α	the metal material's linear expansion coefficient;
β	the temperature coefficient of the change in surface wave velocity with temperature;
V_{RT}	the wave velocity of the ultrasonic surface wave corresponding to the change in elastic modulus;
L_T	the propagation distance of ultrasonic waves at temperature T;

References

1. Zhang, Z.; Xie, K.; Xie, W. Analysis of Existing Steel Structure Bridge Diseases and Research on Protection Technology. *North. Transp.* **2021**, *9*, 14–17.
2. Yue, K.; Xu, L.; Liu, J. Energy dissipation evaluation of butterfly-shaped steel plate shear keys under different loading protocols. *Structures* **2024**, *60*, 105893. [CrossRef]
3. Yue, K.; Xu, L.; Liu, J. Seismic performance of an energy dissipating shear key for highway bridges using butterfly-shaped steel plates. *Eng. Struct.* **2023**, *295*, 116885. [CrossRef]
4. Tong, K.; Zhang, H.; Zhao, R.; Zhou, J.; Ying, H. Investigation of SMFL monitoring technique for evaluating the load-bearingcapacity of RC bridges. *Eng. Struct.* **2023**, *293*, 116667. [CrossRef]
5. Hagara, M.; Trebuňa, F.; Pástor, M. Analysis of the Aspects of Residual Stresses Quantification Performed by 3D DIC Combined with Standardized Hole-drilling Method. *Measurement* **2019**, *137*, 238–256. [CrossRef]
6. Li, R.; Xu, L.; Zhang, S. Application of Residual Stress High-Speed Drilling Method in Thick-Walled Pipeline Steel Pipes. *Phys. Test.* **2019**, *37*, 1–5.
7. Zhang, H.; Ma, X.; Jiang, H. Grading Evaluation of Overall Corrosion Degree of Corroded RC Beams via SMFL Technique. *Struct. Control Health Monit.* **2023**, *2023*, e6672823. [CrossRef]
8. Zhang, H.; Qi, J.; Zheng, Y. Characterization and grading assessment of rebar corrosion in loaded RC beams via SMFL technology. *Constr. Build. Mater.* **2024**, *411*, 134484. [CrossRef]
9. Rainieri, C.; Fabbrocino, G. Development and validation of an automated operational modal analysis algorithm for vibration-based monitoring and tensile load estimation. *Mech. Syst. Signal Process.* **2015**, *60*, 512–534. [CrossRef]
10. Bonopera, M. Stress Evaluation in Axially Loaded Members of Masonry Buildings and Space Structures: From Traditional Methods to Combinations with Artificial Intelligence Approaches. *Buildings* **2023**, *13*, 2097. [CrossRef]
11. Wang, G.; Liao, L.; Zhang, S. Laser Ultrasonic Detection of Concrete Stress under the Influence of Stress History. *Sci. Technol. Eng.* **2021**, *21*, 14734–14741.
12. Liu, H.; Liu, T.; Li, Y. Ultrasonic Measurement Method of Residual Stress on Metal Material Surfaces. *J. Mech. Eng.* **2021**, *57*, 118–125.
13. White, R.M. Generation of Elastic Waves by Transient Surface Heating. *J. Appl. Phys.* **1963**, *34*, 3559–3567. [CrossRef]
14. Zhan, Y.; Zhang, E.; Ge, Y. Residual Stress in Laser Welding of TC4 Titanium Alloy Based on Ultrasonic laser Technology. *Appl. Sci.* **2018**, *8*, 1997. [CrossRef]
15. Zhan, Y.; Liu, C.; Zhang, J. Measurement of residual stress in laser additive manufacturing TC4 titanium alloy with the laser ultrasonic technique. *Mater. Sci. Eng.* **2019**, *762*, 138093. [CrossRef]
16. Zhan, Y.; Li, Y.; Zhang, E. Laser ultrasonic technology for residual stress measurement of 7075 aluminum alloy friction stir welding. *Appl. Acoust.* **2019**, *145*, 52–59. [CrossRef]
17. Xue, M. Research on Non-Destructive Detection of Residual Stress in Metal Surfaces Based on Laser Ultrasonics. Master's Thesis, Zhejiang University, Hangzhou, China, 2018.
18. Ye, C.; Ume, I.C.; Zhou, Y. Inspection of the residual stress on welds using laser ultrasonic supported with finite element analysis. *Manuf. Rev.* **2019**, *6*, 3. [CrossRef]
19. Pan, Z.; Song, J.; Gao, Y. Residual Stress Measurement of GH4169 Superalloy Based on Laser Ultrasonic Method. *Chin. Q. Mech.* **2021**, *42*, 98–107.
20. Ji, B.; Cao, J.; Huang, G. Research on Laser Ultrasonic Guided Wave Detection Method for Internal Stress in Steel Plates. *Chin. J. Lasers* **2022**, *49*, 7–15.
21. Ji, B. Research on Laser Ultrasonic Detection Method for the Composite Quality of Metal Laminated Plates. Ph.D. Thesis, University of Science and Technology Beijing, Beijing, China, 2022.
22. Qian, Z.; Han, X.; Wang, G. Laser Ultrasonic Detection of Residual Stress on the Surface of K417G Turbine Disk after Shot Peening. *Appl. Laser* **2022**, *42*, 91–95.
23. He, X. Research on Nondestructive Testing of Residual Stress in Metal Components Based on Laser Ultrasonics. Master's Thesis, North University of China, Taiyuan, China, 2024.
24. Sampath, S.; Zhang, Z.; Tham, Z.; Chen, Y.; Seng, D.; Gantala, T.; Zhang, L. Non-contact measurements of residual stress distribution and grain size in titanium alloys with laser ultrasonic system. *Int. J. Mech. Sci.* **2024**, *264*, 108809. [CrossRef]
25. Wang, Y. Numerical Study on Laser Ultrasonic Detection of Surface Cracks on Shafts. Master's Thesis, Dalian University of Technology, Dalian, China, 2019.
26. Truesdell, C. Book Review: Finite deformation of an elastic solid. *Bull. Am. Math. Soc.* **1952**, *58*, 577–580. [CrossRef]

27. Bompan, K.F.; Haach, V.G. Ultrasonic tests in the evaluation of the stress level in concrete prisms based on the acoustoelasticity. *Constr. Build. Mater.* **2018**, *162*, 740–750. [CrossRef]
28. Xu, S. Stress Identification of Steel Components Based on Ultrasonics and Deep Learning. Master's Thesis, Hunan University, Changsha, China, 2022.
29. Wang, G.; Liao, L.; Zhang, Z. Laser Wakefield Electron Acceleration and Novel Radiation Sources. *Sci. Technol. Eng.* **2021**, *21*, 14734–14741.
30. Yu, C.; Qin, Z.; Liu, C. Laser Wakefield Electron Acceleration and Novel Radiation Sources. *Chin. J. Lasers* **2024**, *51*, 0101002.
31. Adin, M.Ş.; Adin, H.; Ergün, R.K. Finite Element Analysis of Safety Pin in Snowplow Equipment. *Eur. J. Tech. (EJT)* **2022**, *12*, 89–92. [CrossRef]
32. Dong, L.; Feng, S.; Zhu, L.; Jiang, H. Research on the Localization and Quantification of Internal Crack Defects in Aluminum Plates Based on Laser Ultrasonics. *Appl. Laser* **2022**, *42*, 102–111.
33. Bai, X. Calculation of Surface Stress Field of Objects Based on Laser Grating Method. Master's Thesis, Beijing University of Chemical Technology, Beijing, China, 2023.
34. Tian, J. Research on Full Focal Imaging Detection of Laser Cladding Layer Defects Using Ultrasonic Phased Array Surface Waves. Master's Thesis, Changsha University of Science & Technology, Changsha, China, 2022.
35. Liang, C. Research on the Interaction between Laser Ultrasound and Metal Defects Based on COMSOL. Master's Thesis, Beijing Jiaotong University, Beijing, China, 2020.
36. Shi, Y.; Shen, Z.; Ni, X. Laser-Excited Rayleigh Wave Measurement of Residual Stress in Aluminum Alloy Welds. *Chin. J. Lasers* **2008**, *10*, 1627–1631.
37. Li, L. Research on the Application of Ultrasonic Nondestructive Testing in Bolt Flaw Detection. Master's Thesis, North China Electric Power University, Beijing, China, 2022.
38. Zeng, Z. *Practical Handbook of Steel Materials*; Mechanical Industry Press: Beijing, China, 2015.
39. Xu, Z.; Fan, Z. Phenomenological Interpretation of the Variation Law of Elastic Modulus of Metal Materials with Temperature. *J. Southwest Jiaotong Univ.* **1993**, *2*, 92–97.
40. Luo, L. Testing of Internal Plane Stress in Metal Materials by Acoustoelastic Effect. Master's Thesis, Jiangsu University of Science and Technology, Zhenjiang, China, 2010.